Catalysis Science & Technology

Accepted Manuscript

ROYAL SOCIETY OF CHEMISTRY

www.rsc.org/catalysis

Journal Name

RSCPublishing

ARTICLE

Synthesis and evaluation of highly dispersed SBA-15 supported Ni-Fe bimetallic catalysts for steam reforming of biomass derived tar reaction

Cite this: DOI: 10.1039/x0xx00000x

Received 00th January 2012,
Accepted 00th January 2012

DOI: 10.1039/x0xx00000x

www.rsc.org/

Y. Kathiraser[a], J. Ashok[a] and S. Kawi[a,*]

Abstract: Highly dispersed Ni-Fe bimetallic catalysts supported on mesoporous SBA-15 were synthesized via incipient wetness impregnation method by impregnation of small amount of oleic acid mixed with metal precursor on SBA-15 support. This catalyst system was then tested for steam reforming of biomass tar reaction. Cellulose was used as a biomass model compound for this reaction. Among the various compositions tested, an optimum catalyst composition of 6Ni-1Fe/SBA-15 gave superior catalytic performance in terms of stability and activity. At 600°C, about 90% of biomass was converted to gaseous products over 6Ni-1Fe/SBA-15 catalyst, which is the highest among all the catalysts tested. From X-ray diffraction analysis, the Ni metal and Ni-Fe alloy crystallite sizes were barely distinguishable due to formation of nano-catalysts less than 3nm in size. The metal particle of less than 3nm in size was further confirmed through TEM analysis. Moreover, temperature programmed reduction studies indicate uniform distribution of bi-metallic Ni-Fe species which possess strong metal support interaction with the mesoporous SBA-15 support. This was also indicated via X-ray photoelectron spectroscopy results. TGA study over spent catalyst shows that all Fe contained catalysts generally has less carbon deposition rates compared to over 7Ni/SBA-15 catalyst.

Introduction

The global demand of energy, finite source of fossil fuel, as well as escalating oil prices have further widened research on renewable resources as sources of fuel [1]. In recent years, research on renewable sources such as biomass (obtained from various abundant sources such as agricultural, forest and municipal solid waste materials) and biomass derived liquid fuels are rapidly growing in importance [2, 3]. The conversion of biomass to synthesis gas and hydrogen leads to decrease in CO_2 emission which is significantly important for the environmental fortification [4]. Synthesis gas (syngas) is an important feedstock in the chemical industry, consisting of hydrogen and carbon monoxide in varying compositions. It can be used in a broad spectrum of chemicals and fuels, such as methanol production and ammonia production, or as a source of pure hydrogen for hydrotreating in refineries [5].

Biomass is a renewable energy resource derived from biological sources such as agricultural residues and municipal wastes. It is recognized as one of the promising solutions for current energy and environmental problems [6]. More importantly, biomass is one of the few renewable energy sources that can be converted into liquid fuels as well as feedstock for the chemical industries [7]. Similar to methane reforming, longer hydrocarbons contained within biomass can be reformed using steam or carbon dioxide when passing through a catalyst.

The specific chemistry of biomass gasification is complex and yet to be fully understood by scientists as it involves a complex network of various reactions [6]. In a gasifier, the vaporized biomass molecules break down into condensable tars, nitrogen products and solid char products at high temperatures [7-10]. The major reactions occurring during gasification include pyrolysis, oxidation, partial oxidation, reduction, steam reforming and water-gas shift reactions for further production of gases such as H_2, CH_4, CO, CO_2, H_2O and other light hydrocarbons. Unlike reforming of simple hydrocarbons such as methane, biomass gasification process usually lead to significant tar formation due to its long carbon chains and is the major obstacle towards its commercialization [6, 9, 11, 12]. Tars are usually made up of heavy aromatic hydrocarbons that have high energy content. This not only reduces the energy content of the product gases, but causes operational problems such as plugging when cooled and condensed. Therefore, tar formation is generally found to be among the most critical issue regarding the utilization of biomass via gasification process and its conversion to valuable products is a key research area. By employing a suitable catalyst downstream of the gasification, tars can be removed and the product gas can be adjusted to give higher proportions of H_2 and CO [12].

Transition metals such as Ni and Co are generally favoured over noble metal catalysts for the steam reforming of biomass tar due to their low cost, convenient accessibility and high catalytic activity [8, 13-17]. Among these transition metals, Ni

is found to possess the most potential especially for the hydrocarbon cracking. Nevertheless, several disadvantages associated with Ni-based catalysts include carbon deposition on the catalyst surface and sintering of the metal Ni^o species which lead to deactivation [3, 18].

In general, the size of the catalyst particle as well as metal-support interaction effects are known to play important role in suppressing carbon deposition. Therefore by optimizing the size of the nanoparticles and the structure of the active sites, the catalytic activity and the performance can be improved [19]. Since carbon deposition only occurs when the metal cluster is larger than the critical size, coking can effectively be prevented by having catalyst size smaller than its critical size [20]. Nanocatalysts are generally preferred as more expensive catalytic elements can be dispersed onto the high surface area supports, reducing the overall costs of catalyst production. To ensure high catalytic activity, having a good support with high surface area and stability is also crucial. Highly dispersed catalysts will prevent coking and sintering of the catalysts while ensuring high catalytic activity.

Many reports have focused on the utilization of alumina supported Ni-based catalysts [21-23]. Besides alumina supported catalysts, silica supports are gaining much importance owing to their advantages of high surface area and affinity towards formation of highly stable nickel silicates with strong metal support interaction [15]. Ordered mesoporous silica SBA-15 is found to be a good support for nickel catalysts with thick walls, large pore diameters, and good hydrothermal stability, even at high temperatures [24]. Unlike other mesoporous supports such as mesoporous alumina, mesoporous silica SBA-15 is more readily synthesized in large quantities with consistently high performance. Moreover, their physicochemical structures allow for high dispersion of the metal catalyst particles onto the support.
To prevent sintering of silica-supported Ni catalysts, oleic acid (OA) has been found to be able to inhibit the agglomeration of the particles in the mono dispersed nano crystals [25]. Mo et al. has initiated the *in-situ* self assembled core shell precursor route for the synthesis of highly dispersed monometallic Ni and bimetallic Ni-Cu catalyst supported on silica for CO_2 (dry) reforming of methane [25] and water gas shift reactions [26] respectively. According to Mo et al. [25], addition of a small amount of OA during co-impregnation of the metal nitrate on catalyst support can, not only increase the dispersion of the catalyst on the support, improving the catalytic activity and performance while preventing coking and sintering.

The activity and stability of nickel catalysts can also be improved by adding secondary metals as promoters such as Mn, Co and Fe [27, 28]. Fe is a good option as a co-catalyst as Fe species are found to possess good redox properties [3, 11]. The addition of Fe to Ni catalysts has been reported by Tomishige and co-workers [5, 29, 30] to enhance the activity for steam reforming due to the formation of intimate Ni-Fe interaction in the Ni-Fe alloy with enriched Fe atoms on the catalyst surface. Moreover, the higher affinity of Fe to oxygen has also been reported to suppress the formation of coke [11]. Ashok and Kawi has also found that by alloying Ni with other metals particularly Fe, the catalytic performance in terms of activity and stability can be improved [11]. Fe has been found to act as a co-catalyst by increasing the coverage of oxygen species during the reforming reaction and suppress coke formation [11, 29]. This is also seconded by Djaidja et al. [31] who suggested that the formation of Ni-Fe alloy helps in stabilizing the catalyst and suppressing coke formation.

Therefore, this research aims to develop highly dispersed Ni and Ni-Fe bimetallic catalysts supported on high surface area SBA-15 using the *in-situ* self assembled core shell precursor technique for application in steam reforming of biomass derived tar reaction with cellulose as the biomass model compound. Various characterization techniques such as X-ray diffraction analysis (XRD), temperature-programmed reduction (TPR), X-ray photoelectron spectroscopy (XPS), Brunauer-Emmett-Teller (BET) surface area analysis via N_2 physisorption, transmission electron microscopy (TEM) and thermogravimetric analysis (TGA) were performed. In addition, we have conducted biomass tar reforming reaction at various temperatures and the best catalyst combination was subjected to long-term stability test. The correlation between the structural behaviour of the catalyst and its catalytic activity in the steam reforming of biomass tar was analysed and discussed as well.

Experimental Section

Catalyst synthesis method

SBA-15 mesoporous support material was synthesized via a modified method published by Zhao et al [32]. Firstly, 4.0g of triblock copolymer P123 [$(EO)_{20}(PO)_{70}(EO)_{20,}$ M_w = 5800] is first dissolved in 30mL of deionized water. At a temperature between 35-40^{o}C, 120mL of 2.0M HCl solution and 8.5g of tetraethyl orthosilicate (TEOS) is added and the solution is constantly stirred for 20 h. The solution was then transferred into a 90 °C in a polypropylene bottle and placed in an oven for another 48 h without stirring to allow crystallization. The solid silica product is then collected from the suspension via vacuum filtration, thoroughly washed with deionized water, and dried in air at 60 °C overnight. Finally, the sample is calcined in air at 550 °C for 8h to obtain the final SBA-15 sample.

Three sets of Ni-Fe bimetallic catalysts of differing compositions (with total metal loading of 7wt%) were synthesized using SBA-15 supports. (1) 6wt%Ni-1wt%Fe/SBA-15 (denoted as 6Ni-1Fe/SBA-15); (2) 5wt%Ni-2wt%Fe/SBA-15 (denoted as 5Ni-2Fe/SBA-15); and (3) 3.5wt%Ni-3.5wt%Fe/SBA-15 (denoted as 3.5Ni3.5Fe/SBA-15). The fourth set of sample contains only the mono-metal Ni with 7 wt% loading on SBA-15 (denoted as 7Ni/SBA-15) is used as a control. Nickel nitrate hexahydrate was used as the nickel precursor while iron (III) nitrate nonahydrate was used as the iron precursor. The *in-situ* self-assembled cores-shell precursor route described in a previous work by our group was used to synthesize the catalysts [25]. In this method, via incipient wetness impregnation technique, a small amount of oleic acid (OA), of a fixed molar ratio of n_{OA}/n_{metal} = 0.3, is added to dissolved nickel hydrate hexahydrates and iron (III) hydrate nonahydrates, and thoroughly mixed before the addition of the SBA-15 support. The samples were left to age overnight and transferred to a 60 °C oven and dried for about 6h with intermittent stirring. The catalyst material was then dried at 100 °C for 12 h in an oven and then was calcined at 700 °C for 4h in a muffle furnace (Elite box chamber furnace, UK).

Catalyst characterization

X-ray diffraction (XRD) is employed to provide information on the crystalline structures and identity of the compounds based on the lattice parameter information. XRD analyses were carried out using the Shimadzu XRD-6000 x-ray diffractometer with the Cu target K-α ray as the X-ray source. The operating conditions were fixed at a current of 30mA and voltage of 40kV with the following slit parameters: divergence slit of 1°; scattering slit of 1°; and receiving slit of 0.30 mm. The scanning range was 20° < 2θ < 80° with a scanning speed of 1.5°/min for fresh catalysts and 0.2°/min for reduced and spent catalysts. The average Ni° crystal size was also determined for the pre-reduced (under H_2 environment at 750°C for 1h) and spent catalysts using the Debye Scherrer equation ($D = \frac{0.9\lambda}{\beta\cos\theta}$) where D is the mean size of the crystalline domain; 0.9 is the dimensionless shape factor; λ is the wavelength of the X-ray; β is the peak width and θ is the Bragg angle.

H_2-temperature programmed reduction (TPR) characterization were performed using a Thermo Scientific TPDRO 1100 series system equipped with thermal conductivity detector (TCD) connected to a moisture trap. 50 mg of the catalyst was subjected to reduction in 5% H_2/N_2 gas mixture and heated to 900°C at a heating rate of 10°C/min to obtain the reduction profiles of the catalysts. The surface area of the catalysts were measured using the Brunauer-Emmett-Teller (BET) method via a Micromeritics ASAP 2020 analyzer at 77K by the nitrogen adsorption and desorption isotherms. Prior to analysis, about 50 mg of the samples were degassed at 350 °C for 8 hours to remove any surface impurities and moisture. The sample cells were immersed into a flask containing liquid nitrogen to maintain at the low temperature of 77.4K throughout the analysis. The catalyst particle sizes and structure is further verified using HRTEM system JEOL JEM-2100F. For fresh samples, the catalyst is first reduced at 700 °C under hydrogen for 1h before dispersing ultrasonically in deionized water. The dispersed catalyst was then spread over perforated copper grids. TEM was also performed on spent catalysts to observe the presence of coking or sintering. Similarly, the spent catalyst is dispersed ultrasonically in deionized water and spread over perforated copper grids for analysis.

X-ray photoelectron spectra (XPS) of the pre-reduced catalysts (700 °C for 1 h in H_2 environment) were obtained via a Kratos AXIS spectrometer with a spatial resolution of 30 μm equipped with an Al Kα (hυ= 1486.6eV; 1 eV = 1.6302 x 10^{-19} J) X- ray source. Prior to spectrum sample fitting, the binding energies of the Ni 2p spectra of the samples were referenced to the standard calibrated value of the adventitious carbon, C 1s hydrocarbon peak at 284.6 eV. The amount of carbon deposition on the spent catalyst from the biomass gasification was subjected to thermal gravimetry coupled with differential thermal analysis (TGA-DTA) using a Shimadzu DTG-60 analyzer. The spent catalyst was placed on an alumina pan located on the electronic balance (equipped with a thermocouple) of the analyser. The sample was then heated in air to a temperature of 900 °C at a ramping rate of 10 °C/min.

Steam reforming of Biomass.

Steam reforming of cellulose (Sigma Aldrich) as a biomass model compound was conducted in a laboratory-scale continuous feeding dual-bed reactor. Based on elemental analysis using PerkinElmer 2400 series II CHNS/O system, the dry weight percentage of cellulose was determined as C 42 ± 1%, H 7 ± 0.5%, O 50 ± 1% and S 1 ± 0.5%.

The detail of the steam reforming of biomass reactor setup is similar to our previous published work [33, 34]. The reactor includes the primary bed for biomass steam gasification and accumulation of solid products such as char and ash. The gaseous products may include tar in vapour form at reaction temperature (600°C). The biomass feeder is vibrated with an electric vibrator to allow continuous feeding. Prior to the reforming test, 150 or 250 mg of catalyst was pre-treated under H_2 stream of 30 mL/min at 700°C for 1 h. Upon reduction, He gas was fed from the bottom of the primary bed reactor via a quartz distributor. At the same time, steam (produced by evaporation of water fed by a HPLC pump) was introduced into the main reactor. The catalysts activity tests were carried out at 600°C and at atmospheric pressure using an average biomass flow of 150 mg/min. An Agilent HP 6890 gas chromatograph equipped with a Carboxen column and a thermal conductivity detector was used to analyse the non-condensable gas product. The carbon-based conversion to gas products was calculated by ''A/B * 100'', where A represents the formation rate of products such as CO + CO_2 + CH_4 and B represents the total carbon supplying rate of biomass. Furthermore, the carbon-containing gaseous products yield was also calculated by the ratio of the formation rate to the total carbon supplying rate of biomass. The yield of coke (from TGA analysis) is calculated by (total amount of deposited carbon)/(total carbon amount in fed biomass). The yield of tar and char is estimated as (100 – Carbon based conversion (%) – coke yield (%)).

Results and discussion

Physicochemical characterization of fresh and reduced catalysts.

Fig. 1 shows the XRD profiles of the mono-metallic nickel and bi-metallic nickel-iron oxides supported on SBA-15 catalysts prepared via the *in-situ* self-assembled core shell precursor route using oleic acid as precursor. NiO diffraction peaks are expected at 2θ = 37.0°, 43.12°, and 62.8° (JCPDS-65-5745) [35]. However with the addition of Fe, the formation of $NiFe_2O_4$ and/or Fe_3O_4 will cause the peak to shift to 2θ = 30°, 35.5°, 37.5°, 43°, 57° and 62° [11]. However, due to the effectiveness of oleic acid that is used in the preparation of the catalysts, probably due to formation of metal oleate species, thus preventing the agglomeration of the particles during calcination as reported by Mo et al. [25], most of the samples do not show any observable peaks from the XRD. Moreover, calcination treatment leads to self-assembly of the metallic oxides resulting in high dispersion and formation of metal particles with core-shell like structure [25]. Likewise in this study, strong indication of small and very well-dispersed Ni and Fe particles on the support is present. Moreover, upon reduction of the catalyst samples at 700°C for 1 h and subjected further to XRD analysis (not shown), the metallic Ni/Ni-Fe bimetallic phases are not clearly distinguishable.

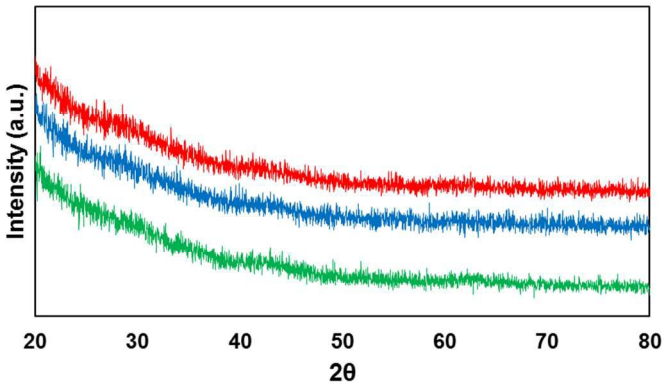

Fig. 1. XRD profile of calcined (a) 7Ni, (b) 6Ni-1Fe and (c) 5Ni-2Fe supported over SBA 15 catalysts.

The morphology of the reduced Ni/Ni-Fe bimetallic catalysts (reduction under H_2 at 700°C for 1h) are shown in the TEM images depicted in Fig. 2. The characteristic hexagonal ordered mesoporous channels of SBA-15 containing the metallic particles within or adjacent to the mesopore walls can be clearly observed. Moreover, TEM images of all the samples show that the particles sizes for all Ni/Ni-Fe range are less than 5 nm, averaging 2-3 nm. These results affirm the small scale of the metallic size indicated from XRD results. Furthermore, to know the distribution of metal species within the catalysts, the reduced 6Ni-1Fe/SBA-15 catalyst was subjected to TEM-EDX analysis (Fig. S1). It can be observed from results that the actual Ni/Fe weight ratios at two different places are 5.32 and 5.45. This result shows that both Ni and Fe species are homogenously distributed all over the catalyst support.

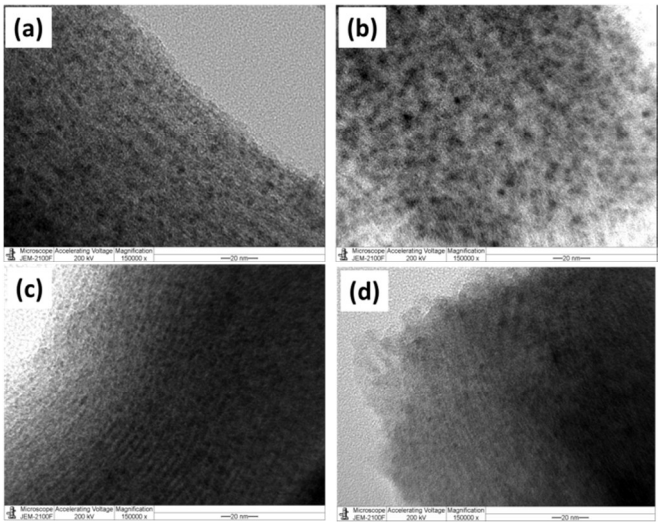

Fig. 2. TEM images of reduced (a) 7Ni, (b) 6Ni-1Fe, (c) 5Ni-2Fe and (d) 3.5Ni-3.5Fe supported over SBA 15 catalysts.

Fig. 3 shows the N_2 adsorption-desorption isotherms at various relative pressures (P/P_0) for each of the catalyst samples obtained from BET analysis. It is observed that the isotherms of the various Ni-Fe/SBA-15 catalysts prepared with oleic acid precursor and calcined at 700°C are type IV Langmuir isotherm with H1 shaped hysteresis loops according to the IUPAC classification [36]. The H1 type hysteresis indicates a complex mesoporous structure in which the network effects are significant [**Error! Bookmark not defined.**] and the addition of promoters could lead to modification or geometric structural changes of the active sites in the metal surface. The physical textural properties of the catalysts are also summarized in Table 1. All the catalyst samples that are tested possess large specific surface area due to the inherent nature of the mesoporous SBA-15 support. In fact, substitution of the Ni metal with only 1wt% Fe resulted in increase in surface area to *ca.* 524m^2. g_{cat}^{-1} compared to the monometallic Ni/SBA 15 catalyst which possessed a surface area *ca.* 505$m^2.g_{cat}^{-1}$. However, further substitution of Ni metal up to 2wt% Fe, did not lead to significant variation in metal surface area and remained similar with the substitution of 1wt% Fe. However, with increase in Fe loading, the pore volume slightly decrease from 0.76 to 0.75. In general, the presence of a larger pore size may reduce the mass transfer resistance to the hydrocarbon feed in the catalysts pore network. Nevertheless the pore diameter slightly decreased with the presence of Fe to *ca.* 6.08 nm compared to 6.18 nm obtained for the un-substituted Ni/SBA-15 catalyst. From these results, it can possibly be deduced that substitution with Fe atoms lead to migration of the metals further within the mesoporous silica host matrix leading to slight contraction of walls [37]. However, since the atomic radii of Fe (126pm) is only slightly bigger than the atomic radii of Ni (124 pm), the difference in pore size is only marginally significant.

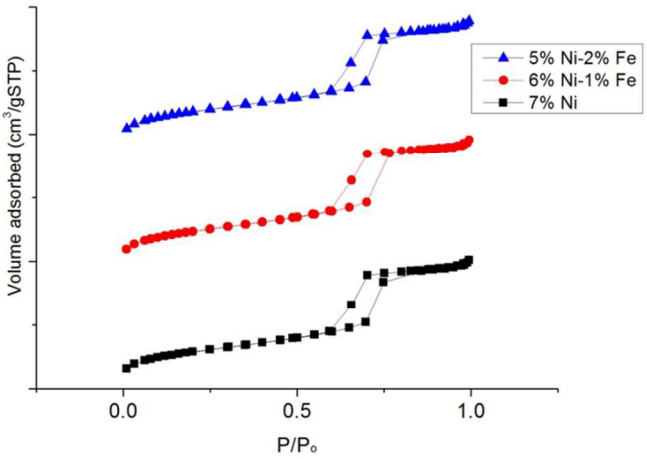

Fig. 3. BET profile of freshly calcined Ni/SBA-15 and Ni-Fe/SBA-15 catalysts.

Table 1: Physicochemical properties of xNi-(7-x)Fe/SBA-15 catalysts

Catalyst Sample	[a]S_{BET} (m^2/g_{cat})	[b]V_p (cm^3/g_{cat})	[c]D_p (nm)
Ni/SBA-15	504.9	0.759	6.17
6Ni-1Fe/SBA-15	523.5	0.760	6.09
5Ni-2Fe/SBA-15	523.4	0.750	6.08

[a]Specific surface area by BET analysis
[b]Total pore volume estimated at $P/P_0 = 0.99$
[c]Average pore diameter calculated by Barrett-Joyner-Halenda (BJH) method

The reducibility profiles of the various SBA-15 supported Ni/Ni-Fe catalysts are illustrated in Fig. 4. The lower

temperature peak (*ca.* 403°C) observed on the monometallic Ni/SBA-15 catalyst correlate to weakly interacting NiO phase with the SBA-15 support, whereas the higher temperature reduction peak *ca.* 603°C relate to stronger metal support interaction between Ni and SBA-15 support. Upon substitution with 1wt% Fe, the 6Ni-1Fe/SBA-15 catalyst displayed a shoulder peak at a lower temperature of 368°C and a singular peak at 615°C. The shoulder peak at the lower temperature region can possibly be attributed to either weakly interacting NiO phase or reduction of iron species, Fe^{3+} to Fe^{2+} (Fe_2O_3 to Fe_3O_4) [38]. It is however, more probable that this shoulder peak relates to the latter, i.e. reduction of iron oxide species. This is because, the 5Ni-2Fe/SBA-15 catalyst also display similar trend, but the peak is more distinct and shifted to even lower temperatures. Hence, this supports the notion that the lower temperature peak is attributed to reduction of Fe^{3+} to Fe^{2+}. The catalyst with only 1wt% Fe showed a higher reduction temperature compared to both the monometallic Ni and bimetallic 5Ni-2Fe supported on SBA-15 catalyst. It has been reported that increase of interaction with Fe species, lead to shift of Ni reduction centres towards higher temperatures [11]. Moreover, since only singular peak exist for the 1wt% and 2wt% Fe substituted catalysts at the higher temperature range (550-650°C), chemical interaction between Ni and Fe such as formation of nickel ferrite is postulated to take place [39]. These results appear to match the deduction of strong metal support interaction indicated by the small particle/crystal sizes based on TEM and XRD analysis.

However, for the equivalent loading of 3.5wt% Ni and Fe supported on SBA-15 catalyst, a broad peak centred at 573°C and another high temperature peak centred at 728°C can be observed. The broad high temperature peak at 728°C can possibly be attributed to the reduction of Fe_3O_4 species to FeO/Fe^0. The broad peak distribution suggests that there may be various nickel and iron phases present in the catalyst. Moreover, the broad width of the high temperature peak suggests the strong interaction between the Ni metal with the SBA-15 support and possible reduction of Fe^{2+} to Fe^o. The postulation on the strong interaction of Ni metal with SBA-15 is further proofed based on XPS results which shall be discussed later. The TPR results indicate that 3.5Ni-3.5Fe/SBA-15 catalyst may not perform as well as the other catalysts due to the broad phase distribution which does not indicate uniformity in dispersion compared to the other catalysts.

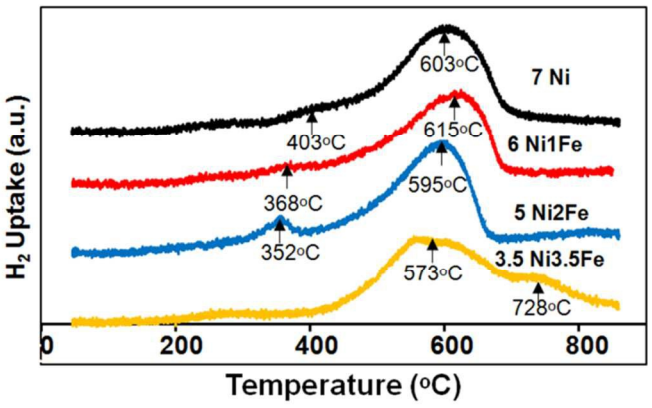

Fig. 4. H_2-TPR profile of the Ni/Ni-Fe supported on SBA 15 catalysts.

Fig. 5 (a) illustrates the Ni $2p_{3/2}$ spectra profiles showing the chemical state of the surface Ni species of the reduced Ni/Ni-Fe supported on SBA-15 catalysts. As tabulated in Table 2, the metallic Ni^0 peak is defined by the characteristic binding energy *ca.* 853 eV [40]. Upon promotion with 1% Fe, a slight shift towards higher binding energy is observed. Similarly, all the peaks from monometallic Ni to Fe promoted bimetallic Ni catalysts exhibit additional Ni^{2+} peak at binding energies ranging between 856-857 eV. All the samples show that a major portion of the Ni species exist in the form of Ni^{2+}. One of the factors includes partial re-oxidation of the sample in air during transfer of samples for analysis in the XPS chamber [41]. Furthermore, Force et al. and Kondarides et al. showed that the existence of strong metal–support interactions on CeO_2-supported catalysts can also be a possible reason behind the existence of Ni^{2+} species in reduced catalysts [40, 42, 43]. This is mainly due to the redox properties of CeO_2-like species; reduced Ni metals can have strong interaction with CeO_2 at the surface and synergistic effects between Ni metals and CeO_2 support can result in a proportion of Ni existing in Ni^{2+} state. Likewise, this phenomenon can also be possible with the Ni/SBA-15 and Ni-Fe/SBA-15 catalysts synthesized *via* the *in-situ* self-assembled core shell precursor route, where stronger interactions between Ni and Si species are inevitable. In fact, the binding energy *ca*. 856.7 eV has been attributed to formation of 2:1 nickel phyllosilicate [44]. However, the major difference observed is that promotion of only 1%Fe led to a slight decrease in terms of metallic state of Ni^0 species to only *ca*. 32% from 36%. However, further increase to 2% Fe, caused a simultaneous shift to the original Ni^0 state along with a greater increase to 49% metallic state. The catalyst with equivalent weight loadings of Ni and Fe, i.e. the 3.5Ni-3.5Fe catalyst displayed an additional peak at even higher binding energy of 859.34, which can be attributed to its incorporation deep within the mesoporous silica walls [45] and possibly formation of 2:1 nickel phyllosilicate as it has the highest binding energy value compared to other reported nickel silicates [45]. In fact, the low Ni loading is a major factor for enhancing the metal support interaction. This phenomenon has also been observed based on the H_2-TPR results which showed a reduction peak at higher temperatures compared to the other catalysts.

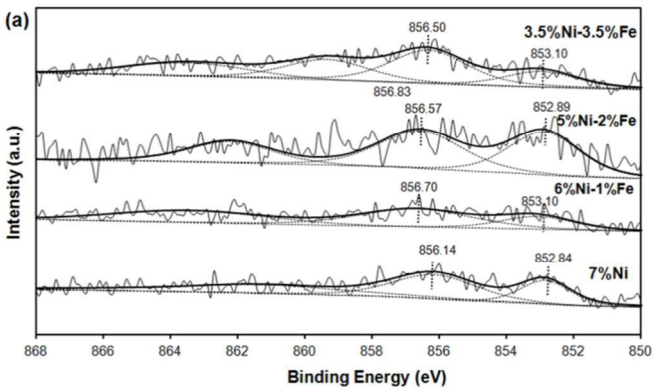

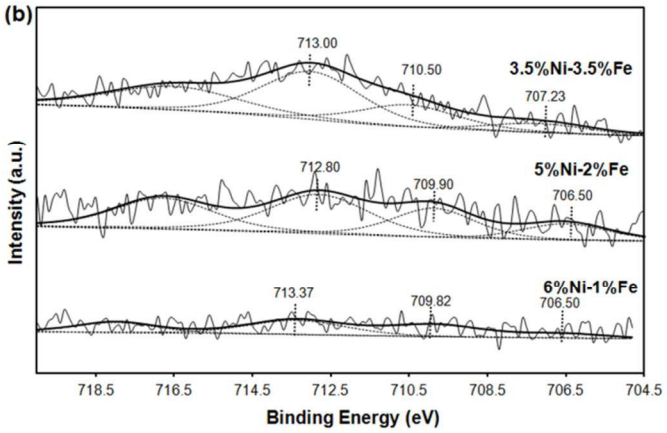

Fig. 5. XPS profile of reduced catalysts: (a) Ni $2p_{3/2}$ spectra and (b) Fe $2p_{3/2}$ spectra.

Table 2: Binding energies of Ni $2p_{3/2}$ and the composition percentage of Ni^{2+} and Ni° of the reduced Ni/Ni-Fe supported on SBA-15 catalysts

Catalyst	Ni $2p_{3/2}$ (Ni°)		Ni $2p_{3/2}$ (Ni^{2+})	
	Ni° (eV)	Ni°/(Ni°+Ni^{2+})	Ni^{2+} (eV)	Ni^{2+}/(Ni°+Ni^{2+})
7Ni/SBA-15	852.84	36.35	856.14	63.65
6Ni-1Fe/SBA-15	853.08	31.82	856.70	68.18
5Ni-2Fe/SBA-15	852.89	48.86	856.57	51.14
3.5Ni-3.5Fe/SBA-15	852.97	20.92	856.32 (859.34)	47.14 (31.93)

Table 3: Binding energies of Fe $2p_{3/2}$ and the composition percentage of Fe^{3+}, Fe^{2+} and Fe° of the reduced Ni-Fe supported on SBA-15 catalysts

Catalyst	Fe 2p3/2 (Fe^0)		Fe 2p3/2 (Fe^{2+})		Fe 2p3/2 (Fe^{3+})	
	Fe^0 (eV)	Fe^0 /Fe	Fe^{2+} (eV)	Fe^{2+} /Fe	Fe^{3+} (eV)	Fe^{3+} /Fe
6Ni-1Fe/SBA-15	706.5	9.9	709.8	39.4	713.4	50.7
5Ni-2Fe/SBA-15	706.5	19.4	709.9	31.0	712.8	49.6
3.5Ni-3.5Fe/SBA-15	707.2	10.1	710.5	30.1	713.0	59.7

On the other hand, as shown in Table 3, promotion with higher amount of Fe (2wt%) led to greater existence of Fe^o in the metallic state, compared to promotion with only 1wt% Fe, which had a greater amount of iron existing in the partially reduced Fe^{2+} state compared to loading of 2wt% Fe. However, the existence of Fe^{3+} (fully oxidized state of iron) is prevalent due to the difficulty of reducing Fe based catalysts [46]. The catalyst with equivalent Ni and Fe loading, showed greatest amount of Fe^{3+} species, which gives indication of its less active nature. Moreover, the binding energy states in the range shown *ca* 712-713 eV, is also indicative of a possible presence of Fe_3O_4 species with Ni-Fe alloy formation, indicated by shift of binding energy towards lower binding energy in Fe 2p spectra and shift towards higher binding energy in Ni 2p spectra [2]. The existence of greater amount of Fe in reduced Fe^o state for all bimetallic catalysts, except for 1wt% Fe loading, correlates with the higher activity displayed by the 6Ni-1Fe catalyst due to the Ni rich Ni-Fe alloy state of elements. Furthermore, the lower amount of metallic state species further show that there is potential for sustained activity over prolonged periods of time taking note of the oxygen scavenging properties induced by Fe introduction.

Steam reforming of cellulose activity.

The Ni-Fe bimetallic catalysts were subjected to steam reforming of biomass derived tar with cellulose as the model compound at 600ºC for 60 min. Fig. 6 shows the amount of cellulose conversion to gaseous products and the H_2/CO ratio of the catalysts with varying Ni-Fe ratio. From the figure, it can be observed that the conversion increases with the addition of Fe. The mono-metallic catalyst (7Ni/SBA-15) performed the lower with only around 70% conversion. 6Ni-1Fe/SBA-15 performed the best out of the 4 with around 90% conversion, suggesting that Fe is effective at low concentrations and its effectiveness in catalyzing the reaction decreases as Fe concentrations increases. This is likely due to the oxygen scavenging effect of Fe (owing to its redox properties), which can effectively promote carbon gasification, whilst providing sufficient active metal site exposure for improved gasification activity. Furthermore, it is probable that Ni-rich Ni-Fe alloy formation is the main active site catalyzing the reaction. However, excessive Fe (above 1wt%) loading proved to be slightly detrimental to the catalytic activity, since the conversion values were lower. This could be due to the overall low active metal loading of 7wt%, of which Ni rich Ni-Fe alloy play a dominant effect in catalyzing the reaction.

In terms of H_2/CO ratio, all 4 catalysts give a ratio of around 1. This is due to the low steam over carbon ratio of only 0.5, which is less than those in literature, which usually range *ca* 3-4. However, the mono-metallic 7Ni/SBA-15 catalysts shows significant drop in the ratio after 30 min, indicating the buildup of carbonaceous species, and further promotion of water gas shift reaction, resulting in lower H_2 formation.

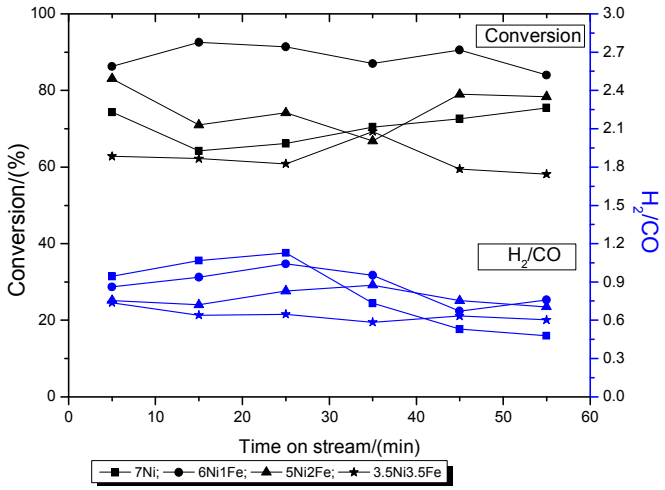

Fig. 6: Biomass conversions to gaseous products and product H_2/CO ratio during steam reforming of biomass tar at 600°C.

Fig. 7 shows the breakdown of the carbon products over 7Ni/SBA-15 and Ni-Fe/SBA-15 catalysts in the steam reforming of cellulose together with steam gasification of cellulose without catalyst at 600°C. Coke from carbon deposition on the catalysts may lead to its deactivation and a decrease in its performance over time [5], while condensable tar and char are heavy hydrocarbons that can pose severe operational problems downstream [12]. Therefore, it is important that a good catalyst can minimize the formation of coke as well as tar's. Based on Fig. 7, for the reaction without catalyst, the carbon based yield from the formation of CO, CO_2 and CH_4 were much lesser compared to that with the catalysts. The formation rate of hydrogen was also much lower than the catalyst and with a H_2 to CO (H_2/CO) value of 0.23. Another important point to highlight is that the yields of char + tar were higher without any presence of catalysts. This result shows the importance of catalyst in reducing the formation of tars and improving the quality of product gases. Furthermore, the mono-metallic 7Ni/SBA-15 catalyst shows significant amounts of tar + char products and significantly higher amounts of coke as compared to the lower doped Ni-Fe bimetallic catalysts. This shows that the addition of an optimum amount of Fe is effective in suppressing carbon deposition on the catalysts, as well as reducing tar formation due to its redox nature.

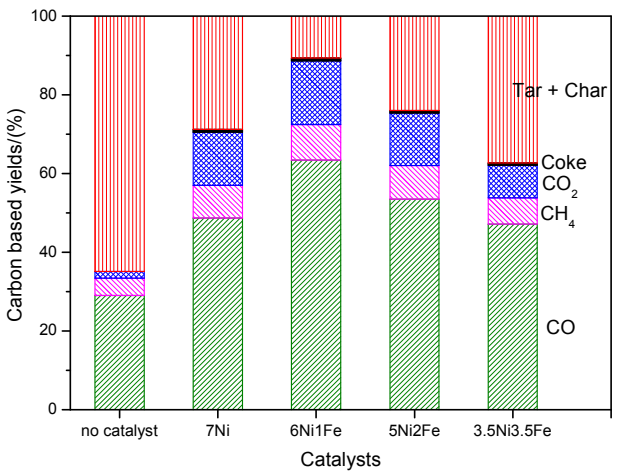

Fig. 7. Product composition (%) in terms of carbon breakdown after steam reforming of biomass tar at 600°C.

The steam reforming of biomass derived tar performances between 7Ni/SBA-15 and 6Ni-1Fe/SBA-15 were further compared in terms of stability with longer reaction times. Fig. 8 shows that the changes of formation rates of H_2, CO, CO_2 and CH_4 with reaction time at 600 °C. Fig. 8(a) depicts the stability performance of 7Ni/SBA-15 catalyst for 180 min. It shows that the formation rates for H_2 and CO_2 are decreasing in trend while the formation rate of CO is increasing in trend with reaction times. As a result the H_2/CO values are varied from 1.1 to 0.7 with time progress. This phenomenon might be related to the catalysts deactivation. On the other hand, for 6Ni-1Fe/SBA-15 catalyst (Fig. 8(b)), the formation rates of H_2, CO, CO_2 and CH_4 gases are nearly same although the reaction time has been increased to 180 min with H_2/CO values above 1.0. It is also observed that the formation rates of H_2, CO and CO_2 gases are significantly higher for 6Ni-1Fe/SBA-15 than 7Ni/SBA-15 catalyst at all reaction times. Thus, these results indicate that the catalytic performance of 7Ni/SBA-15 catalyst in terms of activity and stability can be further improved by replacing some amount of nickel with iron to form Ni-Fe alloys uniformly distributed over SBA-15 support. The thus formed alloy species promotes both steam reforming of tars and water gas shift reactions to reduce the tars formation and enhance H_2 gas production, respectively, during steam reforming of tar derived from cellulose reaction.

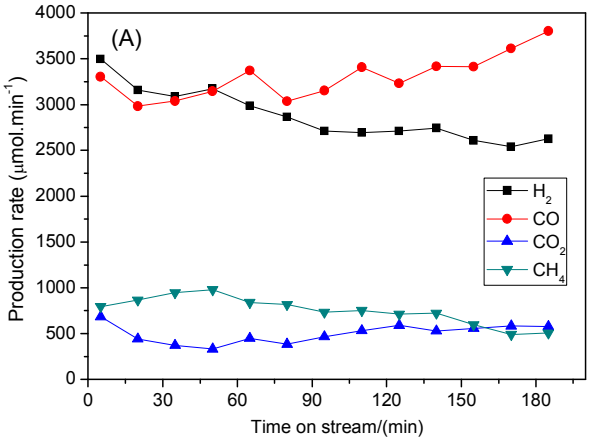

Catalysts	Carbon Deposition Rate (mg_c/g_{cat}-h)
7Ni/SBA-15	510
6Ni-1Fe/SBA-15	193
5Ni-2Fe/SBA-15	187

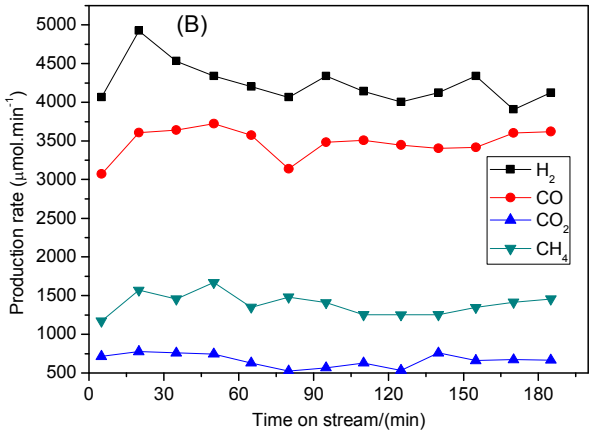

Fig. 8. Changes of catalytic performances in steam reforming of biomass with time on stream over (a) 7Ni/SBA 15 and (b) 6Ni-1Fe/SBA 15 catalysts. Reaction condition: W = 250 mg; α-cellulose = 150 mg.min-1; He = 90 mL.min-1; S/C = 0.5; reaction temperature = 600 °C; reduction temperature = 700 °C/1 h.

Characterization of spent catalysts.

The amount of coke formed from the reaction is analyzed using the DTA/TGA analysis on spent catalysts after gasification reactions at 600°C for 60 min. The results from the TGA analyses are shown in Table 4 as well as Fig. 9. As mentioned previously, monometallic Ni- based catalysts showed the lower catalytic performance as well as greatest amount of carbon deposition of 510 $mgC/g_{cat.}h$. However by replacing just 1-2wt% of the Ni metal content with Fe, the carbon deposition rate can be drastically reduced by up to 2.5 times. This shows the beneficial promoting effect of Fe in the biomass gasification reaction. Most of the DTA profiles in Fig. 9 exhibit one exothermic peak *ca*. 450-550°C. These peak relate to the more reactive amorphous carbon species which can be easily gasified in air [47, 48]. This implies, that the experimental conditions were not sufficiently harsh in promoting formation of the more inert carbon nanotubes. However, the 7%Ni loaded catalyst, displayed an additional shoulder peak *ca*. 340°C, and this could relate to the superficial carbonaceous species on the catalyst, and is likelihood due to the high content of tar and char accumulated in the short reaction period.

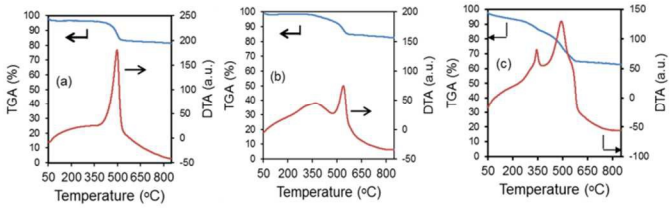

Fig. 9. Results from DT/TGA analysis of spent catalysts after steam reforming of biomass derived tar at 600°C for 1 h reaction time.

Table 4. Carbon deposition rate of spent catalysts after biomass gasification

XRD profile of the spent catalysts is shown in Fig. 10. The Scherrer equation was applied to calculate the approximate crystal size of the spent catalysts. The calculated Ni and/or Ni-Fe alloy crystal sizes for 7Ni/SBA-15, 6Ni-1Fe/SBA-15 and 5Ni-2Fe/SBA-15 are 2.56, 2.62 and 3.57nm, respectively. Corresponding to the observed results from XRD profiles as discussed in the previous section for the reduced catalyst, the samples remain largely similar in size, with only a small amount of sintering, which is more evident for the 6Ni-1Fe/SBA-15 catalyst. However, as mentioned earlier, the limitations of crystallite size determination via XRD can only give us a superficial estimation.

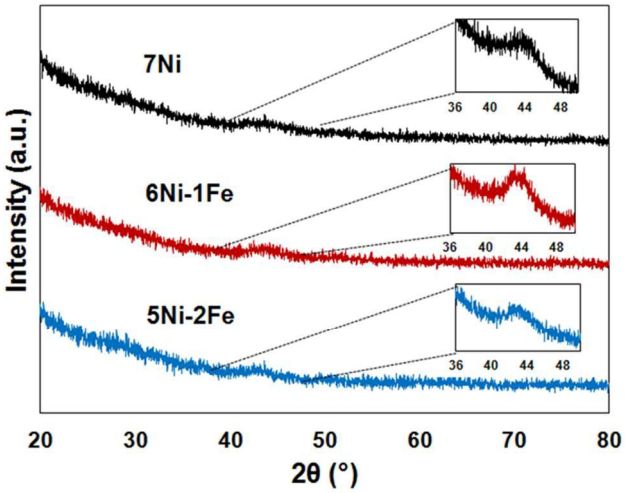

Fig. 10. XRD profile of spent catalyst after reaction during steam reforming of biomass derived tar at 600°C for 1 h reaction time

Fig. 11 (a) displays the Ni $2p_{3/2}$ binding energies of the spent Ni/Ni-Fe supported on SBA-15 catalysts. Two kinds of Ni 2p binding energies at 853.7 eV (Ni^0) and 856.7 eV (Ni^{2+}) were observed for spent 7Ni/SBA-15 catalyst. The former Ni 2p binding energy seems to be slightly shifted to higher value as compared with Ni 2p binding energy of reduced 7Ni/SBA-15 catalyst (Fig. 5(a)). This Ni 2p binding energy is further shifted to higher value for both spent Ni-Fe/SBA-15 catalysts (Fig. 11 (a)). This shift is possibly due to enhanced interaction between Ni and Fe species to form Ni-Fe alloys during reforming reaction. There is no significant change observed for the latter Ni 2p binding energy between Fig. 5(a) and Fig. 11(a). Next, the Fe 2p3/2 binding energies for spent Ni-Fe/SBA-15 was displayed in Fig. 11 (b). Two main Fe 2p binding energies at ~ 705 and ~ 712 eV were observed for both spent catalysts. By combining these binding energies with that of Fig 5(b), it can be observed that both binding energies in spent catalysts are slightly shifted to lower values. This shift is more obvious for the binding energies corresponding to Fe^0 species. This result further confirms the possible enhancement of interaction of Fe species with Ni species in spent Ni-Fe/SBA-15 catalysts.

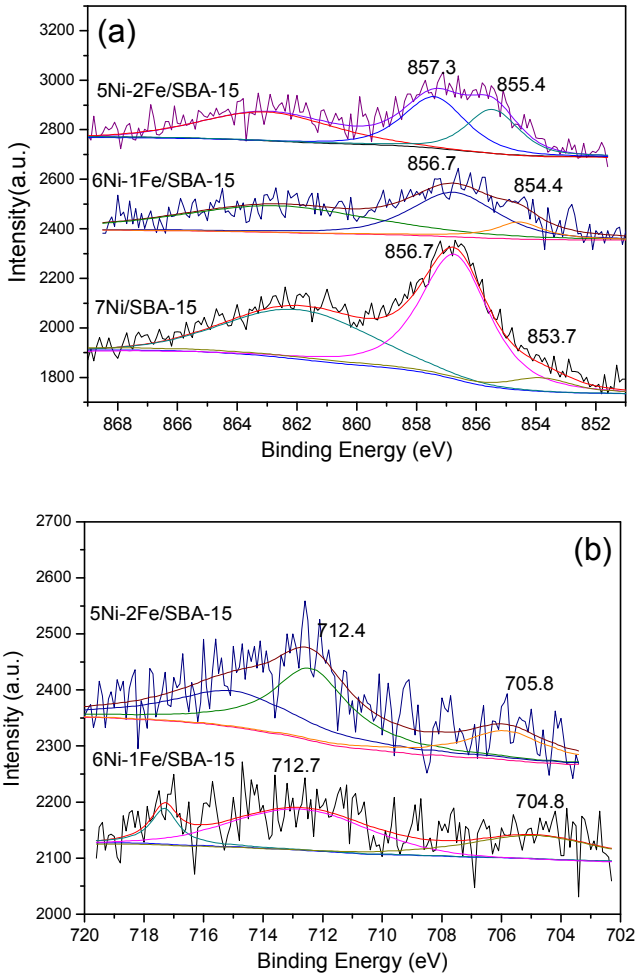

Conclusions

In this study, the performance of monometallic Ni supported on SBA-15 has been compared the bimetallic Ni-Fe supported on SBA-15 catalysts for steam reforming of tar derived from gasification of cellulose (as model biomass compound). The oleic acid assisted incipient wetness impregnation method was used in order to prepare highly dispersed Ni/Ni-Fe supported on SBA-15 catalysts. In fact, the biomass gasification process requires lower steam to carbon ratio, and can be operated at lower temperatures, which is crucial in maintaining catalytic performance of SBA-15 supported catalysts. It was found that the addition of Fe is effective in suppressing carbon deposition rate by up to 2.5 times due to the oxygen scavenging effect of Fe (owing to its redox properties), which can effectively promote carbon gasification, whilst providing sufficient active metal site exposures for improved gasification activity. However, excessive Fe (above 1wt%) loading has proven to be slightly detrimental to the catalytic activity probably due to the overall low active metal loading of 7wt%, of which Ni rich Ni-Fe alloy play a dominant effect in catalyzing the reaction.

Moreover, stability tests conducted for 180 min duration confirms the advantage in introduction of small amount of Fe to the Ni/SBA-15 system, since the formation rates of H_2, CO, CO_2 and CH_4 gases were maintained throughout the stability test with H_2/CO values above 1.0. In addition the product formation rates are significantly higher for 6Ni-1Fe/SBA-15 than 7Ni/SBA-15 catalyst at all reaction times. Hence, the introduction of iron to form uniformly distributed Ni-Fe alloys over SBA-15 support was found to positively promote both steam reforming of tars and water gas shift reactions to reduce the tars formation and enhance H_2 gas production during the biomass gasification reaction.

Acknowledgements

The authors gratefully thank National University of Singapore and National Environmental Agency and Faculty Research Council (NEA-ETRP Grant No. 1002114 and RP No. 279-000-333-490) for generously supporting this work. Y. Kathiraser and J. Ashok, sincerely thanks Dr Oemar Usman and Mr. Yee Jiunn for technical support and discussions.

Notes and references

[a]*Department of Chemical and Biomolecular Engineering, National University of Singapore, Singapore 119260, Republic of Singapore.*
Tel.: +65 6516 6312; fax: +65 6779 1936.
E-mail address: chekawis@nus.edu.sg (S. Kawi).

[1] S. Abelló, E. Bolshak, D. Montané, Appl. Catal. A: Gen., 2013, 450, 261.
[2] J. Ashok, S. Kawi, Appl. Catal. A: Gen. 2015, 490, 24.
[3] U. Oemar, M.L. Ang, W.F. Hee, K. Hidajat, S. Kawi, Appl. Catal. B: Environ., 2014, 148–149, 231.
[4] T. Kimura, T. Miyazawa, J. Nishikawa, S. Kado, K. Okumura, T. Miyao, S. Naito, K. Kunimori, K. Tomishige, Appl. Catal. B: Environ., 2006, 68, 160.
[5] L. Wang, D. Li, M. Koike, S. Koso, Y. Nakagawa, Y. Xu, K. Tomishige, Appl. Catal. A: Gen., 2011, 392, 248.
[6] F.L. Chan, A. Tanksale, Renewable and Sustainable Energy Reviews, 2014, 38, 428.
[7] G.W. Huber, S. Iborra, A. Corma, Chem. Rev., 2006, 106, 4044.
[8] J. Mazumder, H.I. de Lasa, Appl. Catal. B: Environ., 2015, 168–169, 250.
[9] C. Pfeifer, H. Hofbauer, Powder Technol., 2008, 180, 9.
[10] H. Watanabe, D. Li, Y. Nakagawa, K. Tomishige, M.M. Watanabe, Bioresource technology. 2015, 191, 452.
[11] J. Ashok, S. Kawi, ACS Catal., 2014, 4, 289.
[12] D. Sutton, B. Kelleher, J.R. Ross, Fuel Process. Technol., 2001, 73, 155.
[13] J. Nishikawa, T. Miyazawa, K. Nakamura, M. Asadullah, K. Kunimori, K. Tomishige, Catal. Commun., 2008, 9, 195.
[14] S. Irmak, M. Kurtuluş, A. Hasanoğlu, O. Erbatur, Biomass and Bioenergy, 2013, 49, 102.
[15] C. Wu, L. Wang, P.T. Williams, J. Shi, J. Huang, Appl. Catal. B: Environ., 2011, 108, 6.
[16] M. Koike, C. Ishikawa, D. Li, L. Wang, Y. Nakagawa, K. Tomishige, Fuel, 2013, 103, 122.
[17] L. Wang, D. Li, M. Koike, H. Watanabe, Y. Xu, Y. Nakagawa, K. Tomishige, Fuel, 2013, 112, 654.
[18] J. Ashok, S. Kawi, Int. J. Hydrogen Energy, 2013, 38, 13938.
[19] J.R. Rostrup-Nielsen, Catal. Today, 2000, 63, 159.
[20] F. Zaera, ChemSusChem, 2013, 6, 1797.
[21] J. Li, R. Yan, B. Xiao, D.T. Liang, L. Du, Environ. Sci. Technol. 2008, 42, 6224.
[22] J. Mazumder, H. de Lasa, Appl. Catal. B: Environ., 2014, 160, 67.
[23] J. Alvarez, S. Kumagai, C. Wu, T. Yoshioka, J. Bilbao, M. Olazar, P.T. Williams, Int. J. hydrogen energy, 2014, 39, 10883.
[24] L. Jiao, J. Regalbuto, J. Catal., 2008, 260, 342.
[25] L. Mo, K.K.M. Leong, S. Kawi, Catal. Sci. & Technol., 2014, 4, 2107.
[26] L. Mo, S. Kawi, J. Mater. Chem. A, 2014, 2, 7837.
[27] V.M. Gonzalez-DelaCruz, J.P. Holgado, R. Pereñíguez, A. Caballero, J. Catal., 2008, 257, 307.
[28] M. Koike, D. Li, H. Watanabe, Y. Nakagawa, K. Tomishige, Appl. Catal. A: Gen., 2015, 506, 151.

[29] M. Koike, D. Li, Y. Nakagawa, K. Tomishige, ChemSusChem, 2012, 5, 2312.
[30] D. Li, M. Koike, L. Wang, Y. Nakagawa, Y. Xu, K. Tomishige, ChemSusChem, 2014, 7, 510.
[31] A. Djaidja, A. Kiennemann, A. Barama, Stud. Surf. Sci. Catal., 2006, 162, 945.
[32] D. Zhao, J. Feng, Q. Huo, N. Melosh, G.H. Fredrickson, B.F. Chmelka, G.D. Stucky, Science, 1998, 279, 548.
[33] J. Ashok, Y. Kathiraser, M.L. Ang, S. Kawi, Appl. Catal. B: Environ., 2015, 172, 116.
[34] J. Ashok, Y. Kathiraser, M.L. Ang, S. Kawi, Catal. Sci. Technol. 2015, 5, 4398.
[35] Y. Kathiraser, W. Thitsartarn, K. Sutthiumporn, S. Kawi, J. Phys. Chem. C, 2013, 117, 8120.
[36] K.S. Sing, Pure Appl. Chem., 1985, 57, 603.
[37] D. Liu, R. Lau, A. Borgna, Y. Yang, Appl. Catal. A: Gen. 2009, 358, 110.
[38] W. Li, L. Ye, J. Chen, X. Duan, H. Lin, Y. Yuan, Catal. Today, 2015, 251, 53.
[39] M. Pudukudy, Z. Yaakob, Z.S. Akmal, Appl. Surf. Sci., 2015, 330, 418.
[40] J. Kugai, V. Subramani, C. Song, M.H. Engelhard, Y.-H. Chin, J. Catal., 2006, 238, 430.
[41] J.Y. Liu, W.N. Su, J. Rick, S.C. Yang, J.H. Cheng, C.J. Pan, J.-F. Lee, B.-J. Hwang, ChemSusChem, 2014, 7, 570.
[42] C. Force, J.P. Belzunegui, J. Sanz, A. Martínez-Arias, J. Soria, J. Catal. 2001, 197, 192.
[43] D.I. Kondarides, X.E. Verykios, J. Catal. 1998, 174, 52.
[44] Z. Li, L. Mo, Y. Kathiraser, S. Kawi, ACS Catal., 2014, 4, 1526.
[45] D. Liu, X.Y. Quek, W.N.E. Cheo, R. Lau, A. Borgna, Y. Yang, J. Catal., 2009, 266, 380.
[46] K. Polychronopoulou, A. Bakandritsos, V. Tzitzios, J. Fierro, A. Efstathiou, J. Catal. 2006, 241, 132.
[47] C. Querini, Catalysis, 2004, 17, 166.
[48] B.D. Gould, X. Chen, J.W. Schwank, Appl. Catal. A: Gen., 2008, 334, 277.

Graphical abstract: